Journal of Polymers and the Environment (2022) 30:613–621
https://doi.org/10.1007/s10924-021-02218-y

ORIGINAL PAPER

Development of Regenerated Cellulose/Citric Acid Films with Ionic Liquids

Farhad Soheilmoghaddam[1] · Ghorbanali Sharifzadeh[2] · Hossein Adelnia[3] · Mat Uzir Wahit[4]

Accepted: 21 June 2021 / Published online: 3 July 2021

Abstract

Nowadays, the importance of green and biodegradable plastics as viable substitutes for non-degradable petroleum-based materials is felt more than ever. Regenerated cellulose (RC) as a potential candidate suffers from poor processability and inferior properties, limiting its wide applications. In this study, it is demonstrated that citric acid (CA) enhances physical, mechanical, and thermal properties of RC films, due to RC-citric acid compatibility. 1-ethyl-3-methylimidazolium chloride (EMIMCl) as a green ionic liquid was employed for the processing of RC. The optimum properties in terms of thermal stability, mechanical strength, contact angle, water uptake, and oxygen permeability were achieved at 10 wt% of CA. However, further incorporation of CA adversely affected the film properties. This behaviour was explained by the crosslinking and plasticizing effects of CA. Furthermore, in vitro cytotoxicity test demonstrated that RC/CA films are cytocompatible, suggesting the potential advantage of using these biopolymeric films for biomaterial and biological applications.

Keywords Biopolymeric film, Regenerated cellulose · Citric acid · Ionic liquid · Cytotoxicity

Introduction

Regenerated cellulose (RC) as the most abundant renewable resource in nature is considered as a viable substitute for petroleum materials [1, 2]. RC is a linear polysaccharide composed of β-1–4-linked D-glucopyranose repeat units and offers several advantages such as low cost, good biocompatibility, and biodegradability [3]. Despite these, RC has some drawbacks in terms of processability as it can neither be melted due to premature degradation nor be dissolved in common solvents due to strong intra- and inter-molecular hydrogen bonding (H-bonding) alongside its semi-crystalline structure [4]. To address this challenge, various solvent systems such as *N*-methyl morpholine *N*-oxide (NMMO) [5], lithium chloride/1,3-dimethyl-2-imidazolidinone (LiCl/DMI) [6], and phosphoric acid [7] have been employed for the preparation of RC-based materials. However, toxicity, difficult solvent recovery, and possible side reactions of such solvents still remain to be addressed specifically in bio-related areas [8, 9].

Recently, ionic liquids (ILs) as 'green' solvents have attracted a great deal of attention due to their unique features such as negligible vapour pressure, specific solubility, chemical and thermal stabilities, low melting point, and ease of recycling [10–12]. A brief literature survey reveals that room-temperature ionic liquids, especially imidazolium-based, are one of the most promising ILs for wood dissolution [13, 14]. Typically, 1-ethyl-3-methylimidazolium chloride (EMIMCl) is regarded as the most frequently used IL for the preparation of cellulose solutions due to its low toxicity and low reactivity [15, 16].

Despite addressing the processability issue, cellulosic materials typically suffer from inferior properties. One emerging strategy to tackle this issue is the inclusion of a suitable multifunctional compound. Citric acid (CA) can be regarded as a promising biocompatible candidate as it has

✉ Farhad Soheilmoghaddam
m.soheilmoghaddam@uq.edu.au

1 Tissue Engineering and Microfluidic Laboratory, Australian Institute for Bioengineering and Nanotechnology, The University of Queensland, Corner of Cooper and College Road, Queensland 4072 Brisbane, Australia

2 Department of Polymer Engineering, Faculty of Chemical Engineering, Universiti Teknologi Malaysia (UTM), 81310, Johor, Malaysia

3 Australian Institute for Bioengineering and Nanotechnology, University of Queensland, Brisbane, Australia

4 Center for Composites, Universiti Teknologi Malaysia (UTM), Johor 81310 Skudai, Malaysia

one hydroxyl and three carboxyl groups in the structure and widely exists in citrus fruits [17]. The presence of such functional groups can potentially lead to the formation of strong H-bonding, thereby crosslinking the polymer, improving the properties, and adjusting the hydrophilicity [18]. CA has been reported to function as a non-toxic crosslinking agent for poly(vinyl alcohol) [19], starch [20], as well as cyclodextrin-grafted cellulose [21]. Furthermore, CA is employed for the synthesis of cellulose hydrogels through the formation of ester bonds between the polymer chains of cellulose derivatives via anhydride formation [22, 23].

With this background, it is hypothesized that the introduction of CA into RC may ameliorate the properties through crosslinking, making it more versatile for a broader range of applications. To evaluate this hypothesis, a set of RC/CA films were successfully prepared using EMIMCl as a green solvent. The effect of different concentrations of CA was comprehensively assessed on hydrophilicity, oxygen (O_2) permeability, biocompatibility, mechanical, thermal, and morphological properties of the RC films. The results showed that the prepared biopolymeric films may be considered as useful candidates in food packaging, and drug delivery.

Experimental

Preparation of Regenerated Cellulose/Citric Acid (RC/CA) Films

The solution-casted RC films consisting of different concentrations of CA (0, 5, 10, 20 wt% with respect to RC) were produced by adding the CA (Sigma, analytical grade) in the EMIMCL (Sigma, analytical grade) ionic liquid for 20 min after which RC powder (Avicel type, Sigma, powder size of 50 µm and DP of 350) was added. To dissolve RC in EMIMCL ionic liquid, the mixture was heated at 90 ºC for 24 h with constant stirring. The ratio of EMIMCL/RC was 94/6 (wt%). The solution was degassed in a vacuum oven and then cast on a glass plate. The plates were then immersed in a distilled water at room temperature for 12 h to remove the solvent, and then dried under vacuum at 40 ºC for 2 h [24]. The thickness of the films was measured with a digital micrometre and found to be ca. 30 ± 2.35 µm. All the dried films were stored in a moisture-controlled desiccator for further testing. As summarized in Table 1, the films prepared with different CA content (0, 5, 10, 15, and 20 wt%) were coded as RC, RC/CA5, RC/CA10, RC/CA15, and RC/CA20, respectively.

Table 1 The amount of different component used for preparation of the RC/CA films

Samples	RC	RC/CA5	RC/CA10	RC/CA15	RC/CA20
RC (gr)	6	5.7	5.4	5.1	4.8
CA (gr)	0	0.3	0.6	0.9	1.2
EMIMCL (gr)	94	94	94	94	94

UV–Vis Spectroscopy (UV–Vis)

The optical transmittance (T_r) of the pure RC and RC/CA films were measured with a UV–vis spectroscope (Shimadzu UV-3101PC, Japan) at wavelengths ranging from 200 to 800 nm.

X-Ray Diffractometry (XRD)

X-ray diffraction (XRD) patterns were obtained using a XRD diffractometer (Rigaku Miniflex II). Patterns with Cu Kα radiation ($\lambda = 0.15406$ nm) at 40 kV and 30 mA were recorded in the region of 2θ from 5 to 70.

Fourier Transform Infrared Spectra (FTIR)

FTIR spectra were recorded using a PerkinElmer Spectrum-GX spectrometer in the range of 400 to 4000 cm^{-1} at a resolution of 4 cm^{-1} and the speed of 0.2 cm^{-1}/s.

Field Emission Scanning Electron Microscopy (FESEM)

The morphology of RC and RC/CA films was investigated by FESEM using a JEOL JSM-6701 F SEM machine operating at an acceleration voltage of 10 kV [25]. The micrographs were taken from the surface of cryo-fractured samples coated with gold.

Thermogravimetric Analysis (TGA)

Thermal analysis of the RC and RC/CA films was determined using a TGA50 (TGA 50 Instruments, USA). The temperature ranged from 30 to 800 ºC with a heating rate of 10 ºC/min under nitrogen.

Water Absorption

Water absorption (WA) test was conducted according to ASTM D570-98. Samples with 76.2 mm × 25.4 mm × 0.03 mm dimensions were dried under vacuum. Then, they were immersed in distilled water at room temperature until they

reach equilibrium. Afterward, the samples were removed from water, weighed and the weight gains were recorded. Five samples were measured from each formulation and the average value was reported. The % weight gain was determined using Eq. (1):

$$WA(\%) = \frac{W_w - W_d}{W_d} \quad (1)$$

where W_d, and W_W are the weights of dry samples (before immersion) and wet (after immersion) respectively.

Contact Angle Measurement

Contact angle values were measured by the pendant drop method with a water drop of 2 µL and an optical contact angle meter SL 100B from Solon Information Technology Co., Ltd. (Shanghai, China) at room temperature and ambient humidity. The reported value is the average of five measurements.

Oxygen (O_2) Permeability

The O_2 permeability rates were measured using a constant pressure system and soap bubble flow meter at 25 ºC with feed gas pressure of 5 bar. The measurement was repeated three times for each sample. The pure gas permeability was calculated using Eq. (2) [26]:

$$p = \frac{l}{A\Delta P}\frac{dv}{dt} \quad (2)$$

where P, Δp, A, l, t, and V are respectively the permeability, pressure difference across films (Pa), effective surface area (12.5×10^{-4} m^2), film thickness (m), permeation time (s), and volume of the permeated gas ($m^3_{(STP)}$).

Mechanical Properties

Tensile properties were measured with a LRX Tensile Testing Machine (Lloyd, USA) according to ASTM D882-10 at a crosshead speed of 10 mm/min with the gauge length of 30 mm. The specimens were cut into strips of 60 mm × 13 mm × 0.03 mm. The experiment was repeated five times and average values were reported.

Cytotoxicity Analysis

The viability of cells attached on the RC and RC/CA samples was determined by the MTT (3-[4,-dimethylthiazol-2-yl]-2,5-diphenyltetrazolium bromide) assay. For the assay, the samples were fixed in a 96-well tissue culture plate (TCP) and were sterilized with UV light and ethanol, then 1 mL of cell suspension containing 2×10^5 cells/well of human skin fibroblasts (HSF 1184) were seeded evenly onto the samples. The culture medium was changed every 2 days. After seeding for 1, 3, and 5 days, 100 µL of MTT (5 mg/mL) solution was added to each well and incubated at 37 °C for 4 h, respectively; after removal of supernatants, 650 µL of dimethyl sulfoxide (DMSO) was added to each well for dissolving the blue formazan crystal, then the solution was transferred to 96-well plates. The absorbance of the contents of each well was measured at 570 nm using an ELISA microplate reader (Bio-Rad, Model 680, USA). A mean value was obtained from the measurement of four test runs.

Results and Discussion

Apparent Film Properties

In general, transparency is a useful criterion to evaluate the compatibility of the different components in a compound. The transmittance spectra of the films were measured in the wavelength range of 200–800 nm, shown in Fig. 1. The optical transmittance of the pure RC film at 550 nm was 99.6 %, and there was no significant difference in transmittance between the RC and the RC/CA films ($p > 0.05$). These results suggest that CA, even at the highest conc. (20 wt%), is highly compatible with the RC matrix due to chemical affinity and strong interaction [27]. Such an affinity prevents CA from phase separation and crystallization which are the main reasons for the absorption of light and thus film turbidity.

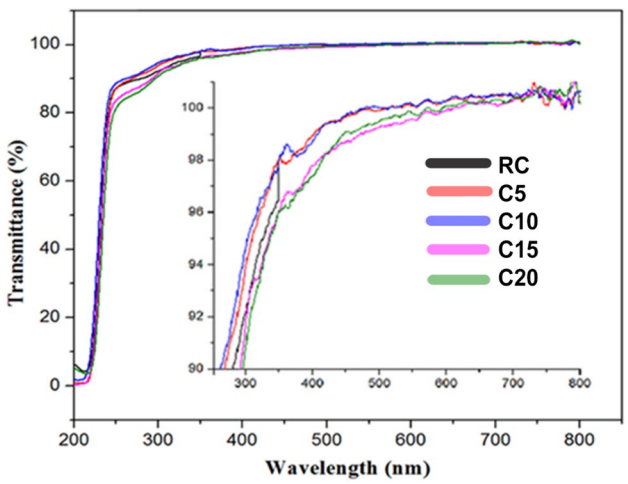

Fig. 1 Light transmittance of RC and RC/CA films, the inset is the magnification of the main graph for transmittance values higher than 90%

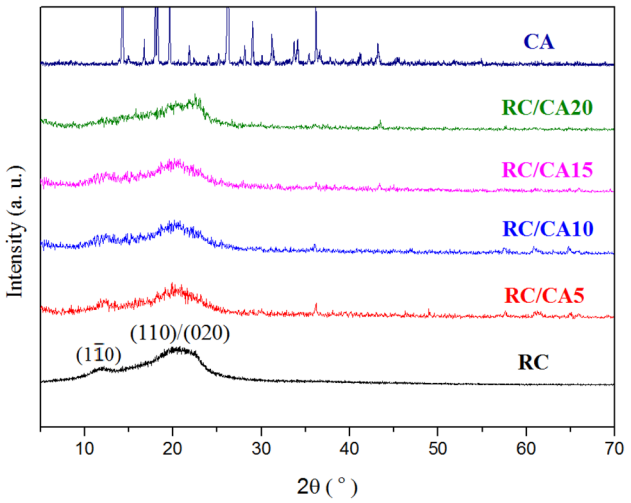

Fig. 2 XRD patterns of CA, RC and RC/CA films

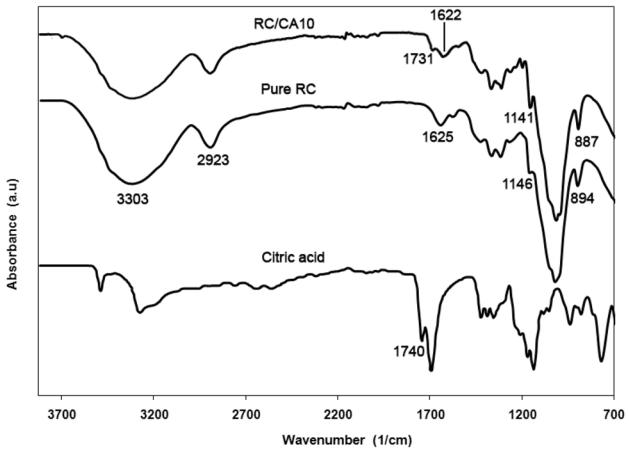

Fig. 3 FTIR spectra citric acid, pure RC, and RC/CA10

X-Ray Diffractometry (XRD)

Figure 2 shows the XRD patterns of CA, RC, and RC/CA films. The RC films exhibited two characteristic peaks at around $2\theta = 12.24°$ and 21.6º which respectively correspond to (1$\bar{1}$0), and (110)/ (020) planes [28]. These peaks are attributed to cellulose I to cellulose II transformation [29, 30]. The diffraction angles of the RC/CA films are almost identical to those of the pure RC. The diffraction peaks of CA which were expected to appear at $2\theta = 14.3º$, 18.2º, 19.6º, and 26.2º were not observed in the diffraction pattern of the RC/CA films (Fig. 2). The disappearance of these peaks may be attributed to the fact that CA is dispersed into the RC matrix in the molecular level, and that RC does not phase separate to form CA crystallite phase within the RC matrix.

To evaluate the effect of CA on the film crystallinity, the diffraction peak at $2\theta = 12.24°$ was compared. The weaker the intensity, the lower the RC crystallinity [31]. As seen, upon the CA incorporation, the intensity of this peak slightly decreased which could be attributed to RC-CA interactions and restricted mobility of RC, leading to a lower chain ordering and crystallinity [32–34].

FTIR Spectroscopy of RC/CA Films

FTIR spectroscopy was employed to determine the existence of any interaction between RC and CA. Characteristic absorption bands of RC are at around 3600–3000, 2923, 1430, 1164 and 894 cm^{-1} (Fig. 3). These absorption bands are ascribed to -OH bond, C-H stretching vibration, CH_2 symmetrical bending, C–O stretching vibration of C–O–H and C-O-C groups, respectively [14]. The most characteristic band of CA which is related to C = O groups is seen at 1740 cm^{-1}. After the CA incorporation, the intensity of the broad peak cantered at around 3300 cm^{-1} was weakened. Furthermore, the presence of CA is proved by the appearance of the peak at around 1731 cm^{-1} (C = O groups of CA) which merged by the band at 1625 cm^{-1} corresponding to C–O stretching vibration of C–O–H of RC. It should also be mentioned that peaks at 1164 and 894 cm^{-1}, which are related to oxygenated groups of RC were slightly shifted to a lower wavelength. The appearance of a new band at 1731 cm^{-1} in the RC/CA10 spectrum could be attributed to free COOH of CA as well as C = O groups of the ester bonds formed as a result of RC-CA crosslinking, as suggested by other researchers as well [35, 36]. Also, the band shifts and broadening of the peak cantered at 1625 cm^{-1}, along with a weaker absorption band at 3303 cm^{-1} could also be due to crosslinking or the formation of H-bonding in the films [37, 38].

Morphology of the RC/CA Films

Figure 4 shows the cross-sectional FESEM images of pure RC and RC/CA20 films. The RC/CA film images displayed a mesh structure, indicating the CA dispersion in the RC matrix at the molecular level. As seen, even at high conc. (20 wt% CA), there is no sign of poor compatibility such as phase separation, drop-matrix morphology, or void formation. Hence, these observations which are also consistent with the XRD results further verify CA-RC compatibility. It can also be seen that the cross-section of RC/CA films is more compact, compared to that of pure RC film, which could be attributed to the physical networks formed as a result of H-bonding [39]. The compact structure of the films as a result of CA bonding with the matrix is responsible for the lower water uptake, lower O_2 permeability, and other improved properties which will be discussed below. Similar observations have been reported for biodegradable citric

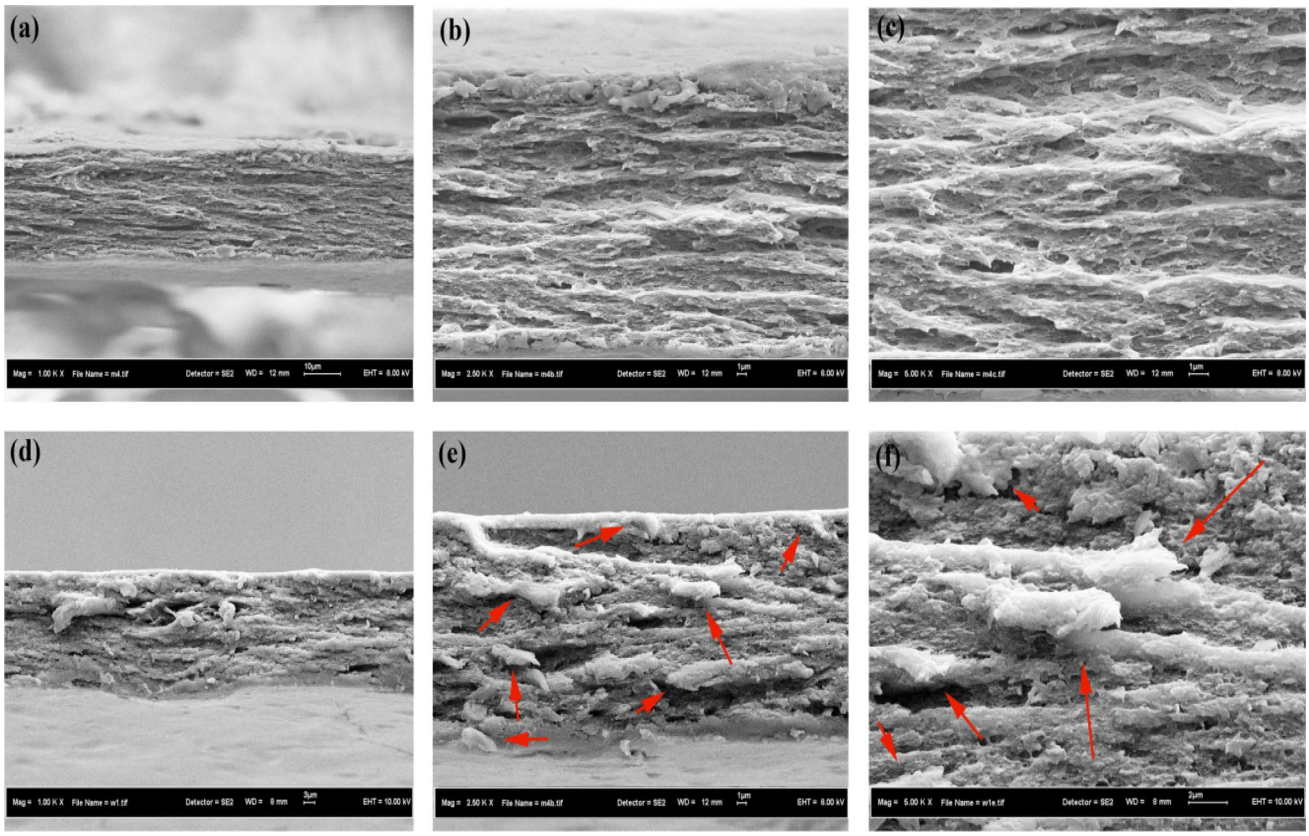

Fig. 4 The cross sectional FESEM images of (**a**–**c**) RC and (**d**–**f**) RC/CA20 films

acid-modified granular starch/thermoplastic pea starch composites [40].

Thermal Stability Analysis

Figure 5 shows the TGA curves of RC and the RC/CA films while Table 2 summarizes the characteristic temperatures. T_{15}, T_{50}, and T_{80} are the temperatures at which 15 %, 50 % and, 80 % of weight loss occurred, respectively [34]. The thermal stability of the films was significantly enhanced by the incorporation of CA especially at high temperatures (> 300 ℃). The T_{80} of the RC/CA10 films increased by 161 ℃ compared to pure RC films. Additionally, the char yields for the RC/CA films improved with CA incorporation up to 10 wt% of CA. The char yield of RC was 12.2 % at 800 ℃, whereas at the same temperature it increased to 17.19 % for the films with 10 wt% CA content. This demonstrates that the increase in CA up to 10 wt% improves the crosslinking, while at the higher contents, its contribution is decreased. Furthermore, the CA decomposition starts from 175 ℃ by decarboxylation. Such decomposition is not noticed in the RC/CA films which further verify the interaction of CA with RC. Citric acid due to good compatibility is able to go between

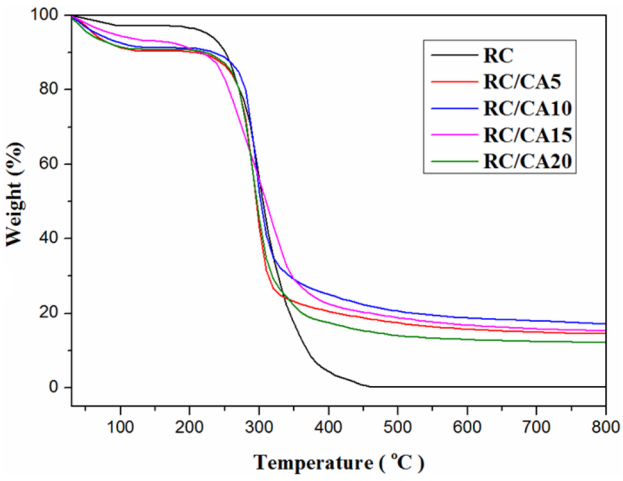

Fig. 5 The TGA curves of RC and RC/CA films

the RC chains and disrupt the intermolecular interactions, thereby forming bonds with the polymer chains. At high concentrations (above 10 wt%), a more open network of H-bonding might be created and results in lower stability (plasticizing effect of CA) [39].

Table 2 TGA results of RC and RC/CA films

Samples	RC	RC/CA5	RC/CA10	RC/CA15	RC/CA20
T_{15} (°C)	262	262	269	262	262
T_{50} (°C)	303	303	310	304	303
T_{80} (°C)	361	427	522	464	423
Residual (%) at 800 (°C)	12.2	15.1	17.19	16.1	14.5

Hydrophilicity of RC/CA Films

The equilibrium water uptake (WA) values of RC and RC/CA films are summarized in Table 3. The highest water uptake was achieved for pure RC films. When CA was added up to 10 wt%, the uptake decreased gradually. The RC/CA film containing 10 wt% CA showed the lowest uptake (WA = 96.8 %). Higher amounts of CA (> 10 wt%) reversed the trend and increased the uptake. This behaviour at low conc. could be attributed to the RC-CA H-bonding and crosslinking effect, restricting the hydrophilic functional groups of RC, while at high conc., the plasticizing effect is the dominant factor, increasing the uptake [39].

Wettability of the films was obtained through the measurement of the contact angle (θ) of a water drop on the films. Images of the liquid drops (distilled water) on the pure RC and RC/CA films are shown in Fig. 6, and the obtained angles are summarized in Table 3. The contact angle of pure RC film was found to be ca. 51.3°, confirming its hydrophilic nature due to the presence of abundant hydroxyl groups [41]. The contact angles increased with increasing CA content. When 10 wt% CA was incorporated, the contact angle value increased to ca. 91.8 ° (Fig. 6). The increase in the contact angle was followed by a decrease when the CA concentration exceeded 10 wt%. The RC/CA10 film exhibited the most hydrophobic characteristic and strongest structure.

As noticed, both water uptake and contact angle values followed a similar trend as they both represent hydrophilicity characteristics of the films. The former and the latter values are considered as bulk and surface hydrophilicity, respectively. The reduction in hydrophilicity of the films at low CA contents (< 10 wt%) is attributed to the reduction of soluble RC content due to RC-CA crosslinking [42]. Involving in such an interaction reduces the accessible number of functional groups for interacting with water both in the bulk and on the surface [43]. Increasing hydrophilicity at a higher amount of CA (> 10 wt%) could be attributed to the CA plasticization effect and presence of excessive amounts of highly polar COOH and OH groups in CA itself [44].

Mechanical Strength

The mechanical properties of films are summarized in Table 3. As seen, the tensile strength and Young's modulus of RC/CA films significantly increased by the incorporation of CA. The tensile strength for the pure RC and RC/CA10 were respectively 35.3, and 66.2 MPa. Young's modulus was also notably increased from 1.8 GPa for pure RC to 3.7 GPa for RC/CA10. Above 10 wt% of CA, however, the mechanical properties decreased slightly. This phenomenon can be explained by the two opposite roles of CA; crosslinking vs. plasticization. The former strengthens the structural integrity through the film and reduces the molecular movements of RC chains, thereby improving the film strength [45]. On the other hand, the latter adversely affects mechanical properties by increasing free volume, lowering chain entanglement, and

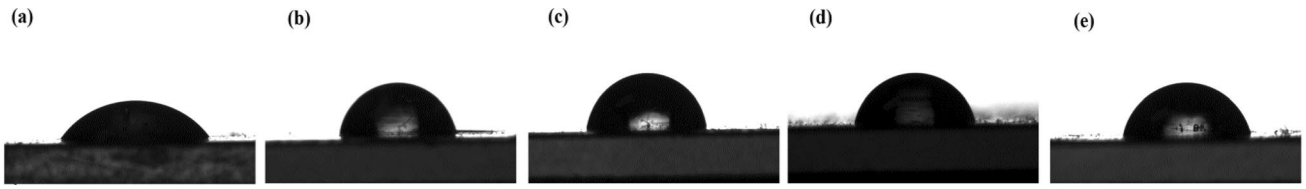

Fig. 6 The contact angle pictures of **a** RC, **b** RC/CA5, **c** RC/CA10. **d** RC/CA15 and **e** RC/CA20

Table 3 Mechanical properties, equilibrium water uptake, contact angle and O_2 permeability of RC and RC/CA films

Samples	Young's modulus (GPa)	Tensile strength (MPa)	Elongation at break (%)	WA (%)	Contact angle (°)	$O_2 \times 10^{-18}$ (m^3 m/m^2 s Pa)
RC	1.8 ± 0.3	35.3 ± 1.2	5.26 ± 0.5	147.7 ± 1.8	51.3 ± 1.8	1.10 ± 0.04
RC/CA5	3.3 ± 0.1	57.4 ± 1.3	6.10 ± 0.3	103.4 ± 1.0	80.5 ± 1.5	0.68 ± 0.04
RC/CA10	3.7 ± 0.3	66.2 ± 1.0	6.28 ± 0.2	96.8 ± 1.4	91.8 ± 1.8	0.55 ± 0.03
RC/CA15	2.8 ± 0.4	48.1 ± 1.5	7.71 ± 0.3	110.3 ± 1.3	76.1 ± 1.1	0.73 ± 0.05
RC/CA20	2.2 ± 0.2	40.4 ± 1.1	8.26 ± 0.4	114.6 ± 1.1	75.7 ± 1.3	0.78 ± 0.03

facilitating the chain motions [39]. Based on the obtained results, It can be concluded that the former is predominant at low CA loading (< 10 wt%), while the latter one prevails at high loadings (> 10 wt%).

Interestingly, the elongation at break of the films improved continuously with CA incorporation and did not follow the trend of modulus and tensile strength (Table 3). It was increased from 5.26 % for pure RC film to 8.26 % for RC/CA20 film. It should be noted that in contrast to covalent attachments, H-bonding interactions are not strong enough to reduce extensibility since they are breakable under stress [46]. Hence, it would be logical to assume that under extension, H-bonds eventually break and RC chains become oriented, thereby improving extensibility [39].

O_2 Permeability

As seen in Table 3, the O_2 permeability of the films decreased dramatically by the addition of up to 10 wt% CA while higher CA content (> 10wt%) reversed the trend. In general, gas permeation through a polymer film is explained by solution diffusion mechanism in which gas permeability (P) is directly proportional to the solubility (S) and diffusivity (D) of the gas in the film ($P = S \times D$) [47]. The former is determined by the polymer/gas molecule chemical affinity, while the latter is determined by the segmental chain motion, free volume, as well as the size and shape of the penetrant molecule. In light of the above results, the permeation reduction at CA < 10 wt% can be attributed to the diffusivity contribution. As a result of RC-CA crosslinking, the molecular motions are hindered, lowering the formation rate of transient gaps (directly related to the extent of free volume). Higher permeation at CA > 10 wt% is however attributed to high free volume arising from the plasticizing effect. It is well understood that the plasticizers improve segmental motions of polymer chains as well as free volume, facilitating the diffusion of gas molecules [39]. It is interesting to note that the trend of mechanical properties is reasonably consistent with that of O_2 permeation.

In Vitro Cytotoxicity Test

The cytotoxicity of RC and RC/CA films was evaluated on human skin fibroblasts (HSF 1184). As shown in Fig. 7, both RC and RC/CA films were cytocompatible. No significant toxicity was observed compared to the control sample. However, a slight improvement was noticed in RC/CA15, and RC/CA20, suggesting that the presence of CA in the films facilitates cell attachment and stimulates cell proliferation. The carboxylic acid and hydroxyl groups CA could contribute to cell binding on films. Furthermore, the CA addition has changed the surface topography and hydrophilicity of the samples which are shown by SEM and contact angle results. Therefore, the rougher surface of RC/CA samples, as well as more hydrophobic characters of RC/CA samples, compared to the RC and control sample has improved the cell adhesion of composites [48]. Cytotoxicity tests using cell cultures have been accepted as the first step in identifying active compounds and for bio-safety testing [49, 50]. Consequently, it can be inferred from the MTT results that all the RC/CA films produced in the present research have the potential to be tested in biomaterials applications.

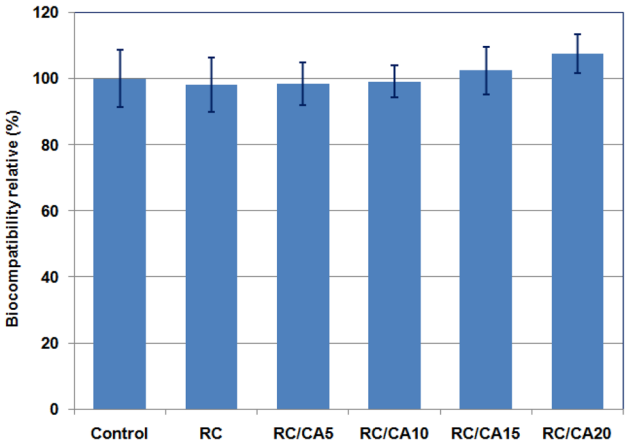

Fig. 7 Cytotoxicity test of RC and RC/CA films on human skin fibroblasts (HSF1184) cell (mean values ± s.e.; n = 3)

Conclusions

Citric acid was successfully incorporated into RC matrix using EMIMCl solvent as a simple and the low cost method. The multi-carboxyl structure of the CA resulted in the interaction between RC and CA. The tensile strength of RC films was remarkably improved by the addition of up to 10 % CA. Citric acid addition also improved the thermal resistance and increased the char residue of RC/CA films. The multi-carboxyl structure of CA could also induce cross-linking which in turn improved the barrier properties and moisture absorption of films. The cytotoxicity results on human skin fibroblast (HSF 1184) cells revealed that the RC/CA films were not toxic and biocompatible. Due to the biocompatibility of RC/CA films with improved oxygen barrier and mechanical properties as well as water resistance properties, these biopolymeric films can be employed as effective replacement for the non-biomaterial derived products with potential in food packaging, membrane, and biomaterials applications.

Declarations

Conflict of interest The authors declare that the research was conducted in the absence of any commercial or financial relationships that could be construed as a potential conflict of interest.

References

1. Soheilmoghaddam M, Pasbakhsh P, Wahit MU, Bidsorkhi HC, Pour RH, Whye WT, De Silva RT (2014) Regenerated cellulose nanocomposites reinforced with exfoliated graphite nanosheets using BMIMCL ionic liquid. Polymer 55(14):3130–3138. https://doi.org/10.1016/j.polymer.2014.05.021
2. Klemm D, Heublein B, Fink H-P, Bohn A (2005) Cellulose: Fascinating biopolymer and sustainable raw material. Angew Chem Int Ed 44(22):3358–3393. https://doi.org/10.1002/anie.200460587
3. Heinze T, Schwikal K, Barthel S (2005) Ionic liquids as reaction medium in cellulose functionalization. Macromol Biosci 5(6):520–525. https://doi.org/10.1002/mabi.200500039
4. Soheilmoghaddam M, Adelnia H, Sharifzadeh G, Wahit MU, Wong TW, Yussuf AA (2017) Bionanocomposite regenerated cellulose/single-walled carbon nanotube films prepared using ionic liquid solvent. Cellulose 24(2):811–822
5. Fink HP, Weigel P, Purz HJ, Ganster J (2001) Structure formation of regenerated cellulose materials from NMMO-solutions. Prog Polym Sci 26(9):1473–1524. doi:https://doi.org/10.1016/s0079-6700(01)00025-9
6. Takaragi A, Minoda M, Miyamoto T, Liu H, Zhang L (1999) Reaction characteristics of cellulose in the LiCl/1,3-dimethyl-2-imidazolidinone solvent system. Cellulose 6(2):93–102. doi:https://doi.org/10.1023/a:1009208417954
7. Northolt MG, Boerstoel H, Maatman H, Huisman R, Veurink J, Elzerman H (2001) The structure and properties of cellulose fibres spun from an anisotropic phosphoric acid solution. Polymer 42(19):8249–8264. doi:https://doi.org/10.1016/S0032-3861(01)00211-7
8. Song H-Z, Luo Z-Q, Wang C-Z, Hao X-F, Gao J-G (2013) Preparation and characterization of bionanocomposite fiber based on cellulose and nano-SiO2 using ionic liquid. Carbohyd Polym 98(1):161–167. doi:https://doi.org/10.1016/j.carbpol.2013.05.079
9. Xiao W, Wu T, Peng J, Bai Y, Li J, Lai G, Wu Y, Dai L (2013) Preparation, structure, and properties of chitosan/cellulose/multi-walled carbon nanotube composite membranes and fibers. J Appl Polym Sci 128(2):1193–1199. doi:https://doi.org/10.1002/app.38329
10. Soheilmoghaddam M, Wahit MU, Tuck Whye W, Ibrahim Akos N, Heidar Pour R, Ali Yussuf A (2014) Bionanocomposites of regenerated cellulose/zeolite prepared using environmentally benign ionic liquid solvent. Carbohyd Polym. https://doi.org/10.1016/j.carbpol.2014.02.085
11. Zhang J, Wu J, Yu J, Zhang X, He J, Zhang J (2017) Application of ionic liquids for dissolving cellulose and fabricating cellulose-based materials: state of the art and future trends. Mater Chem Front 1(7):1273–1290
12. Zhang J, Xu L, Yu J, Wu J, Zhang X, He J, Zhang J (2016) Understanding cellulose dissolution: effect of the cation and anion structure of ionic liquids on the solubility of cellulose. Sci China Chem 59(11):1421–1429
13. El Seoud OA, Koschella A, Fidale LC, Dorn S, Heinze T (2007) Applications of ionic liquids in carbohydrate chemistry: A window of opportunities. Biomacromol 8(9):2629–2647. https://doi.org/10.1021/bm070062i
14. Bendaoud A, Chalamet Y (2014) Plasticizing effect of ionic liquid on cellulose acetate obtained by melt processing. Carbohyd Polym 108(0):75–82. doi:https://doi.org/10.1016/j.carbpol.2014.03.023
15. Lan W, Liu C-F, Yue F-X, Sun R-C, Kennedy JF (2011) Ultrasound-assisted dissolution of cellulose in ionic liquid. Carbohyd Polym 86(2):672–677. doi:https://doi.org/10.1016/j.carbpol.2011.05.013
16. Han J, Zhou C, French AD, Han G, Wu Q (2013) Characterization of cellulose II nanoparticles regenerated from 1-butyl-3-methylimidazolium chloride. Carbohyd Polym 94(2):773–781. doi:https://doi.org/10.1016/j.carbpol.2013.02.003
17. Lee SH, Md Tahir P, Lum WC, Tan LP, Bawon P, Park B-D, Osman Al Edrus SS, Abdullah UH (2020) A review on citric acid as green modifying agent and binder for wood. Polymers 12(8):1692
18. Simões BM, Cagnin C, Yamashita F, Olivato JB, Garcia PS, de Oliveira SM, Grossmann MVE (2020) Citric acid as crosslinking agent in starch/xanthan gum hydrogels produced by extrusion and thermopressing. LWT 125:108950
19. Golabdar A, Adelnia H, Moshtzan N, Nasrollah Gavgani J, Izadi-Vasafi H (2019) Anti-bacterial poly (vinyl alcohol) nanocomposite hydrogels reinforced with in situ synthesized silver nanoparticles. Polym Compos 40(4):1322–1328
20. Gawish S, Ramadan A, Abo El-Ola S, Abou El-Kheir A (2009) Citric acid used as a cross-linking agent for grafting β-cyclodextrin onto wool fabric. Polym Plast Technol Eng 48(7):701–710
21. Ghorpade VS, Yadav AV, Dias RJ (2016) Citric acid crosslinked cyclodextrin/hydroxypropylmethylcellulose hydrogel films for hydrophobic drug delivery. Int J Biol Macromol 93:75–86
22. Demitri C, Del Sole R, Scalera F, Sannino A, Vasapollo G, Maffezzoli A, Ambrosio L, Nicolais L (2008) Novel superabsorbent cellulose-based hydrogels crosslinked with citric acid. J Appl Polym Sci 110(4):2453–2460
23. Adelnia H, Blakey I, Little AMPJ, Ta HT (2019) Hydrogels based on poly (aspartic acid): Synthesis and applications. Front Chem 7:755
24. Hanid NA, Wahit MU, Guo Q, Mahmoodian S, Soheilmoghaddam M (2014) Development of regenerated cellulose/halloysites nanocomposites via ionic liquids. Carbohydr Polym 99:91–97
25. Adelnia H, Gavgani JN, Soheilmoghaddam M (2015) Fabrication of composite polymer particles by stabilizer-free seeded polymerization. Colloid Polym Sci 293(8):2445–2450
26. Soheilmoghaddam M, Wahit MU (2013) Development of regenerated cellulose/halloysite nanotube bionanocomposite films with ionic liquid. Int J Biol Macromol 58:133–139
27. Zhang J, Luo N, Zhang X, Xu L, Wu J, Yu J, He J, Zhang J (2016) All-cellulose nanocomposites reinforced with in situ retained cellulose nanocrystals during selective dissolution of cellulose in an ionic liquid. ACS Sustain Chem Eng 4(8):4417–4423
28. Sharifzadeh G, Soheilmoghaddam M, Adelnia H, Wahit MU, Arzhandi MRD, Moslehyani A (2020) Biocompatible regenerated cellulose/halloysite nanocomposite fibers. Polym Eng Sci. https://doi.org/10.1002/pen.25370
29. Cai Z, Hou C, Yang G (2012) Characteristics and bending performance of electroactive polymer blend made with cellulose and poly(3-hydroxybutyrate). Carbohyd Polym 87(1):650–657. doi:https://doi.org/10.1016/j.carbpol.2011.08.038
30. Li R, Zhang L, Xu M (2012) Novel regenerated cellulose films prepared by coagulating with water: Structure and properties. Carbohyd Polym 87(1):95–100. doi:https://doi.org/10.1016/j.carbpol.2011.07.023
31. Park CW, Lee HJ, Yang Hm W, Ma, Park HG, Kim JD (2011) Size and morphology controllable core cross-linked self-aggregates from poly (ethylene glycol-b-succinimide) copolymers. J Polym Sci Part A: Polym Chem 49(1):203–210

32. Soheilmoghaddam M, Pasbakhsh P, Wahit MU, Bidsorkhi HC, Pour RH, Whye WT, De Silva RJP (2014) Regenerated cellulose nanocomposites reinforced with exfoliated graphite nanosheets using BMIMCL ionic liquid. 55 (14):3130–3138
33. Soheilmoghaddam M, Adelnia H, Bidsorkhi HC, Sharifzadeh G, Wahit MU, Akos NI, Yussuf AA (2017) Development of ethylene-vinyl acetate composites reinforced with graphene platelets. Macromol Mater Eng 302(2):1600260
34. Bidsorkhi HC, Adelnia H, Naderi N, Moazeni N, Mohamad Z (2017) Ethylene vinyl acetate copolymer nanocomposites based on (un) modified sepiolite: Flame retardancy, thermal, and mechanical properties. Polym Compos 38(7):1302–1310
35. Ghorpade VS, Yadav AV, Dias RJJIjobm, (2016) Citric acid crosslinked cyclodextrin/hydroxypropylmethylcellulose hydrogel films for hydrophobic drug delivery. Int J Biol Macromol. 93:75–86
36. Quellmalz A, Mihranyan A (2015) Citric acid cross-linked nanocellulose-based paper for size-exclusion nanofiltration. ACS Biomater Sci Eng 1(4):271–276
37. Gyawali D, Nair P, Zhang Y, Tran RT, Zhang C, Samchukov M, Makarov M, Kim HK, Yang J (2010) Citric acid-derived in situ crosslinkable biodegradable polymers for cell delivery. Biomaterials 31(34):9092–9105
38. Uliniuc A, Hamaide T, Popa M, Băcăiță S (2013) Modified starch-based hydrogels cross-linked with citric acid and their use as drug delivery systems for levofloxacin. Soft Mater 11(4):483–493
39. Lim DBK, Gong H (2018) Highly stretchable and transparent films based on cellulose. Carbohydr Polym 201:446–453
40. Ma X, Chang PR, Yu J, Stumborg M (2009) Properties of biodegradable citric acid-modified granular starch/thermoplastic pea starch composites. Carbohyd Polym 75(1):1–8. doi:https://doi.org/10.1016/j.carbpol.2008.05.020
41. Qiu X, Tao S, Ren X, Hu S (2012) Modified cellulose films with controlled permeatability and biodegradability by crosslinking with toluene diisocyanate under homogeneous conditions. Carbohyd Polym 88(4):1272–1280. doi:https://doi.org/10.1016/j.carbpol.2012.02.007
42. Hashem M, Sharaf S, El-Hady MA, Hebeish A (2013) Synthesis and characterization of novel carboxymethylcellulose hydrogels and carboxymethylcellulolse-hydrogel-ZnO-nanocomposites. Carbohydrate polymers 95(1):421–427
43. Ghanbarzadeh B, Almasi H, Entezami AA (2011) Improving the barrier and mechanical properties of corn starch-based edible films: Effect of citric acid and carboxymethyl cellulose. Ind Crops Prod 33(1):229–235. https://doi.org/10.1016/j.indcrop.2010.10.016
44. Shi R, Bi J, Zhang Z, Zhu A, Chen D, Zhou X, Zhang L, Tian W (2008) The effect of citric acid on the structural properties and cytotoxicity of the polyvinyl alcohol/starch films when molding at high temperature. Carbohydr Polym 74(4):763–770
45. Chen H, Yan X, Feng Q, Zhao P, Xu X, Ng DH, Bian L (2017) Citric acid/cysteine-modified cellulose-based materials: Green preparation and their applications in anticounterfeiting, chemical sensing, and UV shielding. ACS Sustain Chem Eng 5(12):11387–11394
46. Folmer BJ, Sijbesma R, Versteegen R, Van der Rijt J, Meijer E (2000) Supramolecular polymer materials: Chain extension of telechelic polymers using a reactive hydrogen-bonding synthon. Adv Mater 12(12):874–878
47. Adelnia H, Bidsorkhi HC, Ismail A, Matsuura TJS, Technology P (2015) Gas permeability and permselectivity properties of ethylene vinyl acetate/sepiolite mixed matrix membranes. Sep Purif Technol 146:351–357
48. Liu M, Wu C, Jiao Y, Xiong S, Zhou C (2013) Chitosan-halloysite nanotubes nanocomposite scaffolds for tissue engineering. J Mater Chem B 1(15):2078–2089. https://doi.org/10.1039/C3TB20084A
49. Costa-Júnior ES, Barbosa-Stancioli EF, Mansur AAP, Vasconcelos WL, Mansur HS (2009) Preparation and characterization of chitosan/poly(vinyl alcohol) chemically crosslinked blends for biomedical applications. Carbohyd Polym 76(3):472–481. doi:https://doi.org/10.1016/j.carbpol.2008.11.015
50. Adelnia H, Tran HD, Little PJ, Blakey I, Ta HT (2021) Poly (aspartic acid) in biomedical applications: From polymerization, modification, properties, degradation, and biocompatibility to applications. ACS Biomater Sci Eng. https://doi.org/10.1021/acsbiomaterials.1c00150